Batteries & Supercaps

Research Article
doi.org/10.1002/batt.202300332

Chemistry Europe
European Chemical Societies Publishing

www.batteries-supercaps.org

Special Collection

The Role of Surface Coating in P'2-$Na_{0.67}Mn_{0.67}Ni_{0.33}O_2$: Enhancing Capacity and Stability of Layered Cathodes for Sodium-ion Batteries

Gabriele Brugnetti,[a] Nicolò Pianta,[a] Chiara Ferrara,*[a, b] Michele Tribbia,[c] Giorgia Zampardi,[c] Fabio La Mantia,[c] Eider Goikolea,[d] Idoia Ruiz de Larramendi,[d] Luis Lezama,[d] Teofilo Rojo,[d] and Riccardo Ruffo[a, b]

P'2-$Na_{0.67}Mn_{0.67}Ni_{0.33}O_2$ (NMNO) is one of the most promising cathodic materials for new generation sodium-ion batteries (SIBs). One drawback that is preventing its commercialization is however the high instability in the potential window 2.5–4.5 V vs. Na^+/Na, caused by degradation reactions affecting the material's structure and composition. Herein we propose a strategy to overcome this weak spot introducing the surface coating of the material particles with inert magnesium oxide, that has been chosen as coating agent because of its low molecular weight. This protective layer is able to reduce the structural instability of the material without modifying the mixed conduction properties and thus globally stabilizing the electrochemical performances. In fact, the electrode of NMNO coated with 7% of MgO, after an initial stabilization, was able to deliver over 90 mAh g^{-1} of reversible specific capacity at a current value of 50 mA g^{-1}, with a capacity retention of 70% after 250 cycles, to be compared with the 30 mAh g^{-1} of the uncoated material. The effect of the coating on the particles surface is here investigated with differential electrochemical mass spectrometry, to analyze the influence of the treatment on the electrode/electrolyte interphase.

Introduction

The development of new energy storage systems is one of our society's greatest challenges, both for a green energy transition, to manage the inherent unsteady production of renewable energy, and to meet the high energy density, durability, and cost requirements needed for many technological applications. Since their commercialization, lithium-ion batteries (LIBs) have gained particular attention as energy storage devices due to their unique combination of energy and power densities. As a result of this, the market for LIBs has increased year by year and, as shown in Figure 1, is expected to further increase due to the growth of strategic sectors such as the automotive or the grid-based energy storage.[1,2] This is likely to cause sustainability problems in a short term since the abundance of lithium in the Earth's crust is relatively low and its mineral deposits are concentrated in a few limited geographical areas.[3–6] These elements are reflected in the high volatility of raw material prices, which, in cascade, affects the price of batteries. It is thus necessary to find an alternative to LIBs, developing a new generation of sustainable batteries based on highly abundant

[a] Dr. G. Brugnetti, Dr. N. Pianta, Dr. C. Ferrara, Prof. R. Ruffo
Department of Materials Science
University Milano Bicocca
via Cozzi 55, 20125 Milano (Italy)
E-mail: chiara.ferrara@unimib.it

[b] Dr. C. Ferrara, Prof. R. Ruffo
National Reference Center for Electrochemical Energy Storage (GISEL) – INSTM
Consorzio Interuniversitario per la Scienza e Tecnologia dei Materiali
Institution
Via Giusti 9, 50121 Firenze (Italy)

[c] M. Tribbia, Dr. G. Zampardi, Prof. F. La Mantia
Energiespeicher- und Energiewandlersysteme
Universität Bremen
Bibliothekstraße 1, 28359 Bremen (Germany)

[d] Dr. E. Goikolea, Dr. I. Ruiz de Larramendi, Prof. L. Lezama, Prof. T. Rojo
Department of Organic and Inorganic Chemistry
(UPV/EHU) Barrio Sarriena s/n, 48940 Leioa (Spain)

Supporting information for this article is available on the WWW under https://doi.org/10.1002/batt.202300332

Special Collection This publication is part of a joint Special Collection dedicated to Post-Lithium Storage, featuring contributions published in Advanced Energy Materials, Batteries & Supercaps, and ChemSusChem.

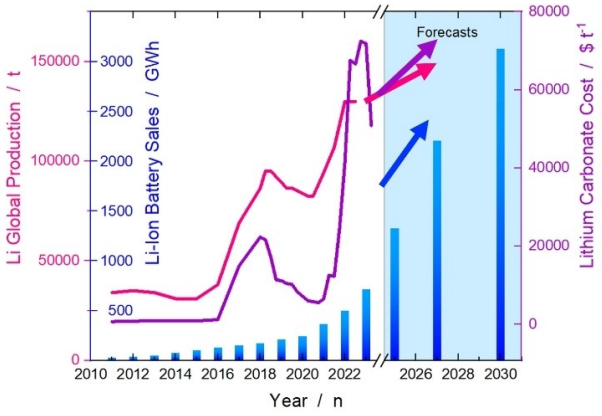

Figure 1. Comparison among Li global production, cost, and demand.[10–13]

and low-cost materials. In this regard, sodium-ion batteries (SIBs) could be a promising alternative to LIBs, as they have similar energy densities, similar electrode reaction mechanisms but less expensive and more sustainable precursors and materials.[7,8] SIBs could replace lithium-ion systems in many applications, especially those where high energy densities are less important, such as stationary applications (grid, back-up, industrial automation, etc.).

To close the performance gap with LIBs and make SIBs more appealing, however, materials with higher performance need to be developed. In particular, the active materials proposed in literature and exploited as positive electrode up to now are characterized by relatively low discharge potentials and discontinuous profiles, limiting the specific energy of the device. Therefore, it is important to develop positive electrodes with adequate specific capacities that are capable of working at high potentials and are formed from abundant elements, also considering that the positive electrode of a LIB accounts for 48 to 52 percent of the total material cost.[9]

Among all the cathodic materials that have been proposed for SIBs application, the most exploited category is the one of layered oxides (TMOs) of general formula Na_xTmO_2 (where Tm represents one or a combination of transition metals) for their similarity with the LIBs system, the easy and scalable synthesis, and the high stability upon cycling. Nickel-containing TMOs, are of particular interest since the Ni redox couples permits to enhance the power density and the average potential of the final device.[14–18] At the same time, one of principal drawbacks of these materials, is the structural instability at high potential (>4.1 V vs. Na^+/Na) that can be attributed to phase transitions and to irreversible redox reactions involving the oxygen anions of the lattice structure due to the peculiar electronic structure of these materials. An emblematic example of this behavior is the P2-$Na_{0.67}Mn_{0.67}Ni_{0.33}O_2$ phase, which exhibits a specific capacity of almost 85 mAh g^{-1} in the voltage region 2.5–4.1 V vs. Na^+/Na, with an excellent stability upon cycling and rate capability. The specific capacity can be doubled (to about 180 mAh g^{-1}) by extending the voltage window up to 4.5 V; nevertheless, in this case the cycling stability is significantly impaired and fades quickly.[19] The reasons for the poor performance are attributed to a partially irreversible P2-O2 phase transition and the peculiar electronic structure of the material, with the bands related to the 2p orbitals of O partially overlapping the d orbitals of the transition metals. Thus, during oxidation, at potentials greater than 4.2 V vs. Na^+/Na, a charge compensation mechanism occurs by irreversible oxidation of lattice oxygen atoms and not by reversible oxidation of Ni or Mn atoms.[20] As a confirmation of this, Zhang et al. recently demonstrated the release of O_2 from the layered structure and the formation of an insulating layer on the particles that affects the subsequent electrochemical process.[21]

To solve the problem of the low-capacity retention at high voltage, two main approaches are proposed in literature: i) to dope the material with other electrochemically active or inactive metal cations, such as Fe or Mg,[21–25] thus increasing the covalency of the Tm–O bond and modifying the electronic structure thus suppressing the O_2 evolution but lowering in some cases the average potential; ii) to protect the surface of the particles with a coating layer, such as with Al_2O_3 or other materials and mechanically stabilizing the materials.[25–31]

Herein, we present a new coating approach performed by a wet chemistry method using magnesium oxide as a coating agent. Two different NMNO samples with 5% and 7% MgO coating are here proposed and fully characterized; the uncoated NMNO material is also presented as a benchmark. The samples were named NMNO_0 (uncoated sample), NMNO_5 and NMNO_7 (coated samples). The coating agent percentages were carefully chosen to obtain a balance between the beneficial effects of the protecting layer and the loss in specific capacity due to the coating agent inert mass. The MgO coating, differently from the approach already used in literature with Al_2O_3, was obtained from a wet chemistry method exploiting ethanol to avoid the water induced Na^+ extraction from the layers of the material and the related worsening of the electrochemical performances, as recently reported.[32] The Mg-based coating agent was chosen because of its low atomic weight, that permits to have a higher amount of coating moieties, more homogeneous and abundant compared with other coating agents with higher molecular mass. The effects of the coating on the cathode material particles were evaluated by means of scanning electron microscopy (SEM) and of X-Ray diffraction (XRD) to determine variations induced by the procedure utilized in the morphology or in the composition and structure of the material. The electrochemical performances of the uncoated and coated material were then evaluated with rate capability test and with long cycling and the beneficial effects of the coating were also evaluated by means of differential electrochemical mass spectrometry (DEMS).

Results and Discussion

The P2-$Na_{0.67}Mn_{0.67}Ni_{0.33}O_2$ material has been synthetized by wet chemistry approach; the co-precipitation synthesis route was chosen because of the high regularity in the final product morphology (single crystal-like) that is generally obtained with this pathway. A regular morphology has been associated with a very high tap density of the cathodic powders, an important aspect for obtaining high energy density electrodes.[33] The synthesis parameters reported in the experimental part (mainly the temperature) were chosen to obtain a P2 phase (according to Delmas' notation[34]), since it's reported for similar materials that this structure presents the best electrochemical properties compared to others, such as for example the O3.[35,36]

XRD diffractograms of the materials (Figure 2a) showed the presence of the characteristic reflections of the desired phase, as at a first glance the pattern of the NMNO is compatible with the reference card JCPDF Card No. 00-054-0894 ($P6_3$/mmc space group). Nevertheless, the Rietveld refinements (Figure 2b) have been based on the use of the P'2 model (C2/m space group), previously reported as a distortion of the P2 structure, to account for extra peaks; results of the refinements are reported in Table 1.[34,37,38] The two structures differ only for small distortion in the Tm–Na positioning within the cell. The crystal

Research Article
doi.org/10.1002/batt.202300332
Chemistry Europe
European Chemical Societies Publishing

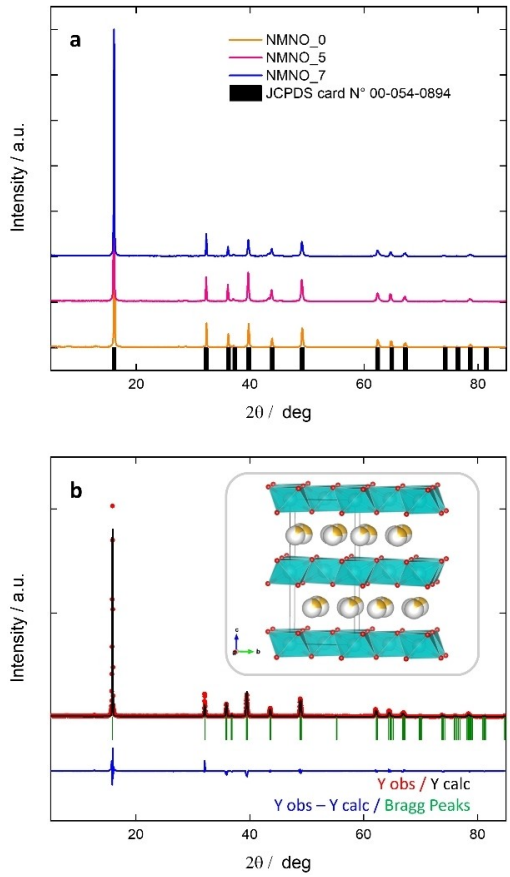

Figure 2. XRD patterns for the NMNO_0 (blue), NMNO_5 (tangerine), NMNO_7 (Schiapparelli pink) samples (a) and Rietveld refinement results for the NMNO_0 sample together with the representation of the layered structure with Mn/Ni octahedra in Tiffany blue, Na in yellow, O in red. Na ions are reported as white/yellow spheres to represent the uncomplete occupation of the crystallographic sites.

structure is composed by TmO_6 (Tm = Mn, Ni) octahedra sharing bridging oxygen ions forming layers along the ab plane; these layers are alternated by other layers of sodium ions along the c axis. Every sodium ion, as described by Delmas' notation, is accommodated in prismatic sites (P), with two MO_2 slabs in the unit cell (inset of Figure 2b). P2 and P'2 structures are generally characterized by high values of the c cell parameter, that reflects a good spacing among the layers of the crystalline structure; a key feature for the fast and reversible Na^+ intercalation and deintercalation process.

The XRD patterns of the coated materials presented the same reflections of the pristine NMNO in terms of position and shape. The absence of shift in peaks position, particularly for the 00 l class of reflection, supports the hypothesis that Mg is not entering into the pristine NMNO structure. No significant extra peaks are observed, neither shift nor broadening of the reflections related to the NMNO material. This implies that i) the P'2 structure is maintained and the coating procedure does not alter the structure; ii) the obtained coating is not highly crystalline. Indeed, due to the high symmetry of MgO, despite its low mass fraction, some reflections could be expected. The absence of reflections associated with MgO can be correlated with its amorphous nature and/or with nanoparticles formation, as discussed in more details in the next paragraph.

The coating homogeneity was evaluated via SEM/EDX analyses. Figures S1 and S2 in the Supporting Information, reported as an example, show that Mg is dispersed all over the NMNO particles, thus proving the homogeneity of the coating.

The structural retention was expected since the temperature at which the coating is performed is in the range of stability of the material. Of particular importance is the fact that the first peak, associated to the 002 family of planes, was not shifting, meaning that the c axis of the cell did not varying. As stated before, the c parameter is strongly correlated with the Na-layers content. Indeed, layered oxides can intercalate molecules or atoms between the TmO's layers, and that can change dramatically the electrochemical behavior of the material .[32,39] The invariance of the c parameters with the coating procedure supports the idea of no Na^+ losses and no intercalation of water/ethanol moieties; the refined cell parameters are reported in Table 1.

No substantial differences were detected both in the cell parameters and in the cell volume of the coated materials, confirming thus that the coating was not affecting the structure of the starting material. As already mentioned, the temperature at which the coating is carried out is far from the synthesis temperature, however, in literature have been reported several materials in which Mg atoms are introduced in the TmO_6 layer during the thermal treatment.[40–43] The refined Na occupancies suggest that no clear dependence on the Na content on the percentage of coating can be outlined; it is in the expected range but slightly lower that the nominal composition. One interesting aspect emerging from the analysis of the refined cell parameters is that the beta angle of the cell is increasing with the content of coating agent. This could mean that the presence of the coating on the particles' surface is inducing a strain of the structure.

To further ensure that in the coating process no diffusion nor doping of magnesium cations towards the layered oxide of the core has taken place, the magnetic response of the NMNO_0 and NMNO_7 samples has been analyzed by electronic

Table 1. Refined cell parameters, Na occupancies, and agreement factors obtained from the Rietveld refinement of XRD data for the NMNO series of samples.

Sample	*a* [Å]	*b* [Å]	*c* [Å]	*β* [deg]	*V* [Å^3]	Na occ.	Chi2	R_{wp}
NMNO_0	2.8800(1)	5.0149(1)	11.1529(5)	90.149(3)	161.08(1)	0.54 (8)	17.2	26.3
NMNO_5	2.8787(1)	5.0149(2)	11.1546(5)	90.279(3)	161.05(1)	0.47 (7)	12.4	24.7
NMNO_7	2.8808(1)	5.0149(2)	11.1524(7)	90.326(3)	161.14(1)	0.58 (5)	13.9	20.5

Research Article
doi.org/10.1002/batt.202300332
Chemistry Europe
European Chemical Societies Publishing

paramagnetic resonance (EPR). Figure 3 shows the effect of the MgO coating on the EPR signal, observing that the signal recorded for both samples has the same shape, *g* value and line width. In this way, it is possible to determine that both samples present similar magnetic interactions due to the NMNO material, thus making it possible to rule out the introduction of Mg into the layers of the material. From the intensity of both spectra, a decrease of around 20% is detected when coating the material with MgO (measured from the area under the curve). This behavior is related to a lower magnetic susceptibility in the NMNO_7 sample, which is in good agreement with the presence of a diamagnetic coating such as MgO.

Finally, the analysis of the experimental composition (Table 2) shows that the Na content is lower than expected for all the samples, in good agreement with the trend reported from XRD data. The Mn/Ni ratio on the contrary matches the desired composition. Finally, the MgO content can be estimated in 0, 4.0, and 5.6 moles per unit formula for the NMNO_0, NMNO_5, and NMNO_7 samples, respectively, confirming the effectiveness of the Mg based introduction.

The morphology of the as-prepared material was constituted of extremely regular single crystal-like particles,[44,45] characterized by very smooth surfaces, a morphology that can be obtained with specific synthesis routes[46,47] and it is highly desirable for the intercalation of ions (Figure 4a, b).[45,48] The particles presented a tablet-like shape, with a particles' height ranging from 1 to 3 μm and width ranging from 1 to 8 μm. The average size is 3.15 μm, as determined from image analysis. The active material particles presented well defined edges, showing in some cases a hexagonal shape, as expected from the crystal structure. For the NMNO_5 and NMNO_7 samples this morphology is preserved (Figure 4c and d), as also the size distribution,

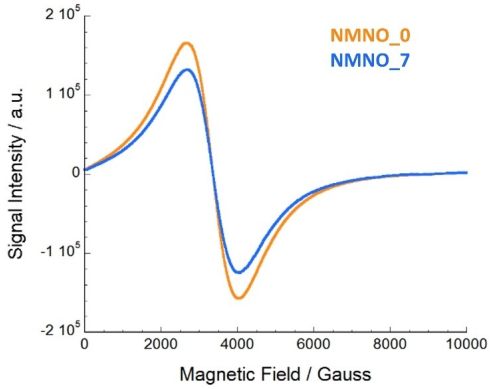

Figure 3. Room-temperature EPR spectra of the NMNO_0 and NMNO_7 samples.

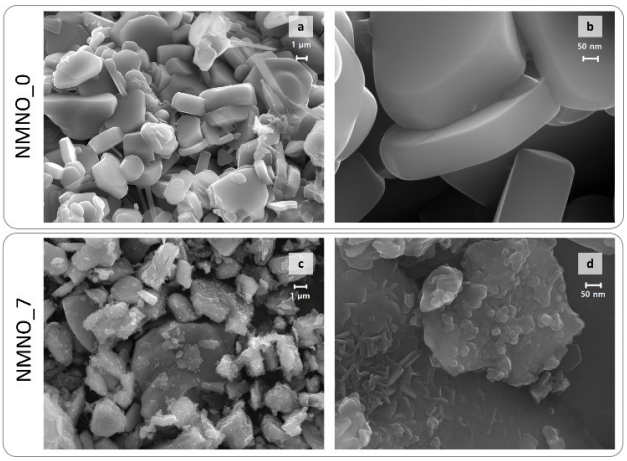

Figure 4. SEM images for a, b) NMNO_0 and c, d) NMNO_7 samples.

while clear differences were observed on the surface of the particles, which presents a wrinkled morphology evidencing the growth of the MgO coating layer. More in detail, the growth of both nanoflakes and granular structures with dimensions below 50 nm was observed on the surface of the coated particles. The low particle size, the possible amorphous nature of the coating and the low percentage, explain the absence of MgO peaks in the XRD pattern.

The micrometric single crystal morphology induced by this synthesis is generally associated with high tap density values.[49,50] The tap density of NMNO_0 (evaluated putting 1 g of material in a 1 mL syringe) resulted to be of 2 g cm^{-3}, which is comparable with either high-tap density literature material and commercial standards for lithium (the tap density of commercial lithium nickel manganese oxide is $\geq$2.1 g cm^{-3}).[50–52] In conclusion, the combination of XRD and SEM analysis demonstrates that the coating was successfully performed on the surface of the active material particles, without affecting neither the structure nor the morphology.

To assess the effect of the coating, systematic electrochemical tests have been performed on the NMNO_0, NMNO_5, and NMNO_7 materials in half-cell configuration. First of all, Electrochemical Impedance spectra have been collected at OCV so to observe the effect of coating on the charge transfer processes. As observed in Figure S3, there are no substantial differences in the spectra collected with NMNO_0 and NMNO_7 as active materials for working electrodes. This suggests that the coating does not affect the charge transfer process in a negative way.

Table 2. Elemental content as % with respect to the nominal composition as derived from ICP analysis (error is within 5%) and comparison among the nominal and experimental compositions.

Sample	Na [%]	Mn [%]	Ni [%]	Mg [%]	Nominal composition	Experimental composition
NMNO_0	83.4	95.9	97.7	0	$Na_{0.67}Mn_{0.67}Ni_{0.33}O_2$	$Na_{0.56}Mn_{0.64}Ni_{0.32}O_2$
NMNO_5	76.4	99.1	102.0	1.6	$Na_{0.67}Mn_{0.67}Ni_{0.33}O_2$ * 5 MgO	$Na_{0.51}Mn_{0.66}Ni_{0.34}O_2$* 4.0 MgO
NMNO_7	76.6	98.1	100.5	2.2	$Na_{0.67}Mn_{0.67}Ni_{0.33}O_2$ * 7 MgO	$Na_{0.51}Mn_{0.64}Ni_{0.33}O_2$* 5.6 MgO

Research Article
doi.org/10.1002/batt.202300332
Chemistry Europe
European Chemical Societies Publishing

Electrochemical measurements were firstly carried out in the voltage range 2.5–4.1 V vs. Na^+/Na by galvanostatic cycling with potential limitation (GCPL), to investigate the coating effect on materials performances. Pristine NMNO (Figure 5a) presents the typical oxidation/reduction profile, composed by four plateaus at 3.1 V, 3.3 V, 3.6 V, and 3.7 V vs. Na^+/Na. The plateaus are associated to the $Ni^{3+/2+}$ redox process and to a "breathing" of the structure, with an expansion on the c layer and a contraction of the *a* axis, as previously reported.[19,20] The specific capacity is around 85 mAh g^{-1} and the average Coulombic efficiency in the first ten cycles is of 99.5% (Figure 5a). The average capacity retention was 99.1, 95.3, 92.6, and 91% at gravimetric currents of 25, 50, 75, and 100 mA g^{-1} (Figure 5d), respectively. Such values were calculated on the ratio between the last cathodic specific capacity value obtained for each gravimetric current and the tenth anodic specific capacity (the last one at 10 mA g^{-1}). The whole data are in perfect agreement with previous reports on the Ni-doped NMO materials.[19,20] The profiles obtained for NMNO_5 and NMNO_7 show slight differences compared to NMNO_0 (Figure 5b and c). While the shape of the two plateaus at 3.1 and 3.3 V remains almost constant, the two higher plateaus are less marked and shifted to higher potentials. This phenomenon, that was already observed in other cases of coated NMNO,[26] can be related to the presence of the electronic insulator MgO on the particle surface, which worsens the kinetics of the electrochemical performances. This broadening, however, does not imply a change either in the specific capacity of the material nor in the stability upon cycling (Figure 4d). Interestingly, the rate capability of the materials was not affected by the presence of the coating and remains very good, at least in the explored current ranges. On the other hand, a variation was in the mean operating potential observed, slightly increasing from 3.44 V vs. Na^+/Na for the uncoated material to 3.47 V for the two coated ones. This data shows how the coating can improve not only the stability of the material (at higher potentials), but also slightly the energy density.

The change in the de-sodiation/sodiation profiles and the variation in the mean operating potentials can be better appreciated and evaluated in the differential capacity plot (Figure 5e). Indeed, in the 3.0–3.5 V range the peaks of the different materials are quite similar, except for the broadening.

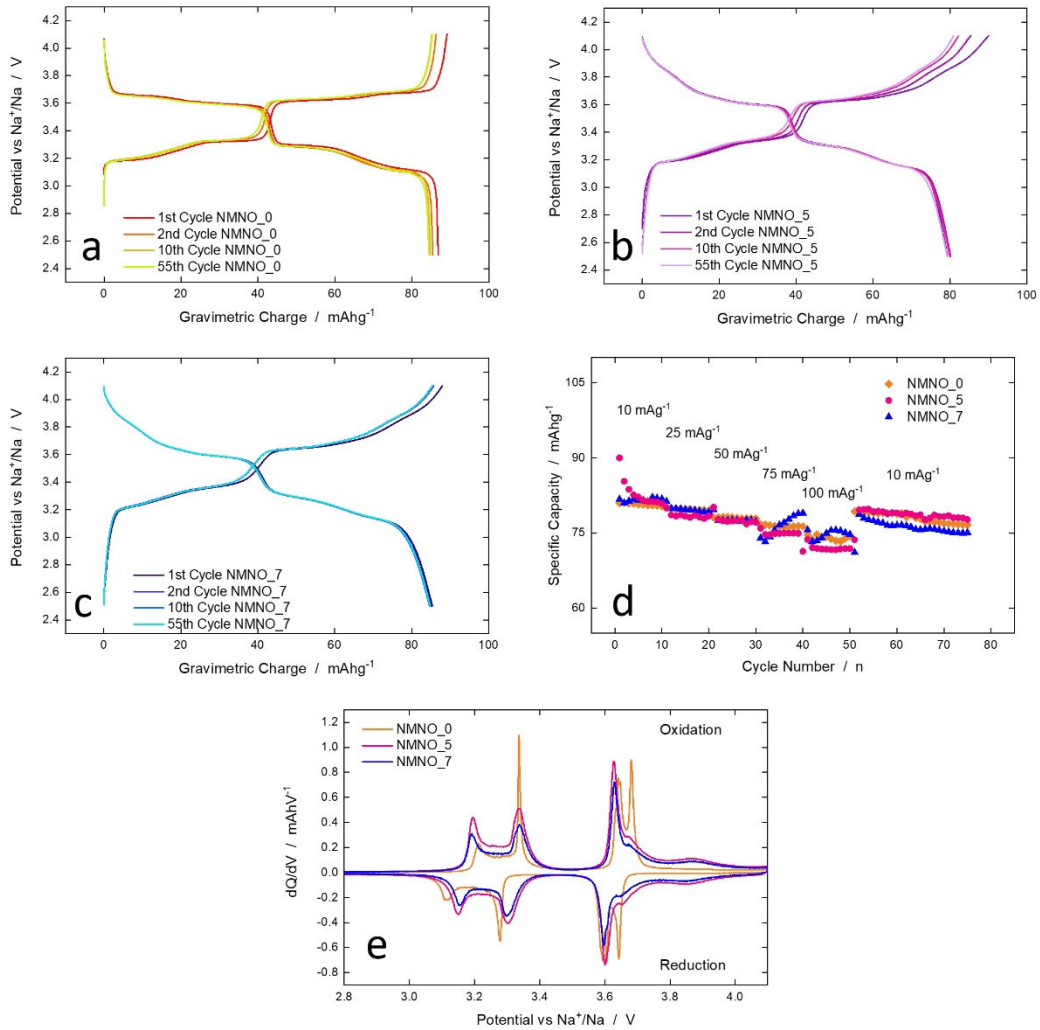

Figure 5. De-sodiation/sodiation profiles of a) NMNO_0, b) NMNO_5, and c) NMNO_7 obtained at 10 mA g^{-1}. d) Anodic specific capacities of the three samples at different current densities, e) differential capacity plot obtained from the first cycle of (a–c).

Only very small differences can be appreciated in the peak positions as in the case of the NMNO_0 reduction peak at 3.11 V that in the NMNO_7 sample is shifted to 3.15 V. Much more evident differences are present in the 3.5–4.1 V potential region: while the first peak (oxidation at 3.64 V, reduction at 3.60 V) remains substantially unchanged, the second changes dramatically. In the uncoated material, the oxidation and reduction peaks are extremely sharp and located at 3.68 V and at 3.64 V, respectively. At these potentials, only small broad peaks are observable in the coated materials, probably related to part of particles not completely covered by the coating layer. On the other hand, in this high potential region, an additional process is present (broad peaks at 3.87 V and 3.85 V in oxidation and reduction, respectively) for the coated samples. This process may likely correspond to the NMNO_0 peak at 3.68 V but shifted at higher potentials by the increase in the overpotential of the electrode due to the insulating coating.

Small variations were observed in the Coulombic efficiencies: the average value of NMNO_5 was 98.4% (less than 99.5% of NMNO_0), whereas the efficiency of the NMNO_7 sample was of 99,2%. A negligible worsening was noticed also in the round-trip efficiency that is of 97% for the uncoated sample and of 95.5 and 96% for NMNO_5 and NMNO_7, respectively.

Overall, these results confirm that the MgO coating did not modify either the peculiar (de)intercalation behavior of the NMNO material or the rate capability when tested in the sharp voltage range 2.5–4.1 V vs. Na^+/Na. On the other hand, small changes were detected in the mean operating potentials.

To assess the effectiveness of the coating, measurements with a broader potential range (from 2.5 to 4.5 V vs. Na^+/Na) were performed. In this case, clear differences among the samples can be detected (Figure 5). The NMNO_0 sample exhibits a first cycle with high specific anodic capacity (213 mAh g^{-1}) but with extremely low Coulombic efficiency (59%). The capacity retention upon cycling is also very low, with a drop to 84 mAh g^{-1} after only 10 cycles, reaching the specific capacity provided by the material in the lower voltage window (Figure 5a). These data are comparable with what reported in literature, where capacity losses of 25% between the first and the second oxidation process are reported.[21] The performance was not stabilized yet after the 75 cycles, meaning how expanding the potential window while testing the uncoated material is not only not convenient, but also detrimental.

The oxidation profile of NMNO_0 in the potential range 2.5–4.5 (Figure 5b), showed the same shape already observed (Figure 5a) plus a new plateau starting from 4.2 V, accounting for an extra capacity of around 115 mAh g^{-1}. This plateau is, as previously stated in the introduction, attributed to sodium ions extraction and charge compensation by a partially irreversible oxidation of the oxygen atoms in the crystalline lattice. The capacity in this region is decreasing cycle after cycle and after just 10 cycles was almost disappeared. During the cathodic half-cycle, the corresponding plateau was at much lower potentials, i.e., between 4.0 and 3.8 V.

This fact can be attributed to the formation of non-conductive degradation products on the particles' surface, which increase the overpotentials of the electrochemical processes. The pristine NMNO_0 tested up to 4.5 V showed also worse kinetic properties compared to the narrow potential range. The observed capacity retention was 78.5, 56.7, 45.7, and 37% at gravimetric current values of 25, 50, 75, and 100 mA g^{-1}, respectively (Figure 5a). A worsening in the capacity retention during the rate test was however expected, since charge compensation mechanism involving oxygen lattice atoms is kinetically slower than the oxidation of transition metal cations.

On the other hand, the NMNO_5 material shows an improved behavior, both in capacity retention and rate capability. The first cycle has a specific anodic capacity of 175 mAh g^{-1} and a Coulombic efficiency of 70%. Even if the initial specific capacity value was lower than NMNO_0, the cyclability was much better (Figure 5a), due to the superior stability induced by the coating. The capacity retention upon cycling was indeed improved, the % values were 84.9, 82.3, 76.8, and 70.8% at the gravimetric currents of 25, 50, 75, and 100 mA g^{-1}, respectively. After 75 cycles, however, the specific capacity trend was not stabilized yet and the obtained value was comparable to that in the lower potential window. The difference between the first cycle anodic capacity of the pristine and NMNO_5 sample is due to the less charge involved in the electrochemical process at the 4.2 V plateau, which was in fact shorter in the coated sample, accounting only for 80 mAh g^{-1}. The de-sodiation/sodiation profiles are also in this case shifting at higher potential cycle by cycle. Thus, for the NMNO_5 sample the effect of the coating was only slowing down the decomposition of the material, probably because the coating layer was not homogeneous enough. This shifting is however not evident in the profiles of the NMNO_7 sample. This material presented an enhanced reversibility of the oxidation/reduction profiles in the larger potential range (Figure 5d). In the first cycle, a specific capacity of 167 mAh g^{-1} was achieved in oxidation with a capacity efficiency of 79%. The capacity retentions observed in the rate test were respectively of 90.3, 80.4, 75.1, and 69.2%, comparable with the other coated material. At the end of the 75 cycles of the measurements, the material was still able to deliver 106 mAh g^{-1}. The uncoated material in the same conditions shows capacity of 62 mAh g^{-1}, whereas the NMNO_5 cathodic specific capacity is of 83 mAh g^{-1}. The NMNO_7 material provides an average operating voltage of 3.66 V, an average coulombic efficiency, (calculated on the final 10 cycles at 10 mA g^{-1}) of 97.82%, and a round trip efficiency of 90.77%, pointing out the very good kinetics of the electrochemical processes.

Overall, the electrochemical properties of MgO coated NMNO compare well with that found in literature for similar systems, both in terms of capacity and capacity retention.[26,27,53] Although there is still room for improvement, the low cost and facile coating procedure makes it potentially interesting for industrial scale applications.

Based on all the aforementioned considerations, the NMNO_7 was selected for long cycling analysis; the material was tested for ten cycles with a gravimetric current of 10 mA g^{-1}, to achieve an initial stabilization, and then increasing the current at 50 mA g^{-1}. The results are compared with the

Research Article
doi.org/10.1002/batt.202300332
Chemistry Europe
European Chemical Societies Publishing

uncoated material (Figure 6e) whose specific capacity was dropping almost immediately under 30 mAh g^{-1}. The coated sample was able to deliver, as the current is set to 50 mA g^{-1} a specific capacity near to 90 mAh g^{-1}, in good agreement with the data previously discussed in Figure 5(a). The specific capacity was well maintained during the measurements. After 250 cycles, in fact, the electrode was still delivering almost 64 mAh g^{-1}, corresponding to a capacity retention (respect to the first specific capacity at this current value) of 70% with a linear capacity loss of about 0.125 mAh cycle^{-1}. At high current the average Coulombic efficiency was of 99.5%.

To have a qualitative demonstration of the suppression of the oxygen release from the material induced by the coating, in-situ differential electrochemical mass spectrometry (DEMS) was performed on the NMNO_0 and the NMNO_7 samples (Figure 7a) at a current value of 25 mA g^{-1} by using a custom cell design validated in previous works.[54,55]

In the first de-sodiation process of the uncoated material at potential values higher than 4.3 V a peak associated to oxygen production was clearly detected from the baseline. Neither this peak, nor the de-sodiation process at the same potentials were observed in the subsequent cycles. Instead, the material exhibited a drastic decay in the specific capacity values, even if the capacity value trend was slightly better than the one exhibited in the coin-cell configuration. While in the first oxidation process the specific capacity reached a high value of 110 mAh g^{-1}, it subsequently dropped in the second and the last cycles to 65 mAh g^{-1} and ~50 mAh g^{-1}, respectively (Figure 6d). Oxygen production was detected only in the first cycle because after the initial oxygen loss the particles of active material are covered by non-conductive degradation products, which prevent the further material decomposition while limiting their electrochemical reactivity.[21] Moreover, it must be stressed out that since the oxygen released during the material

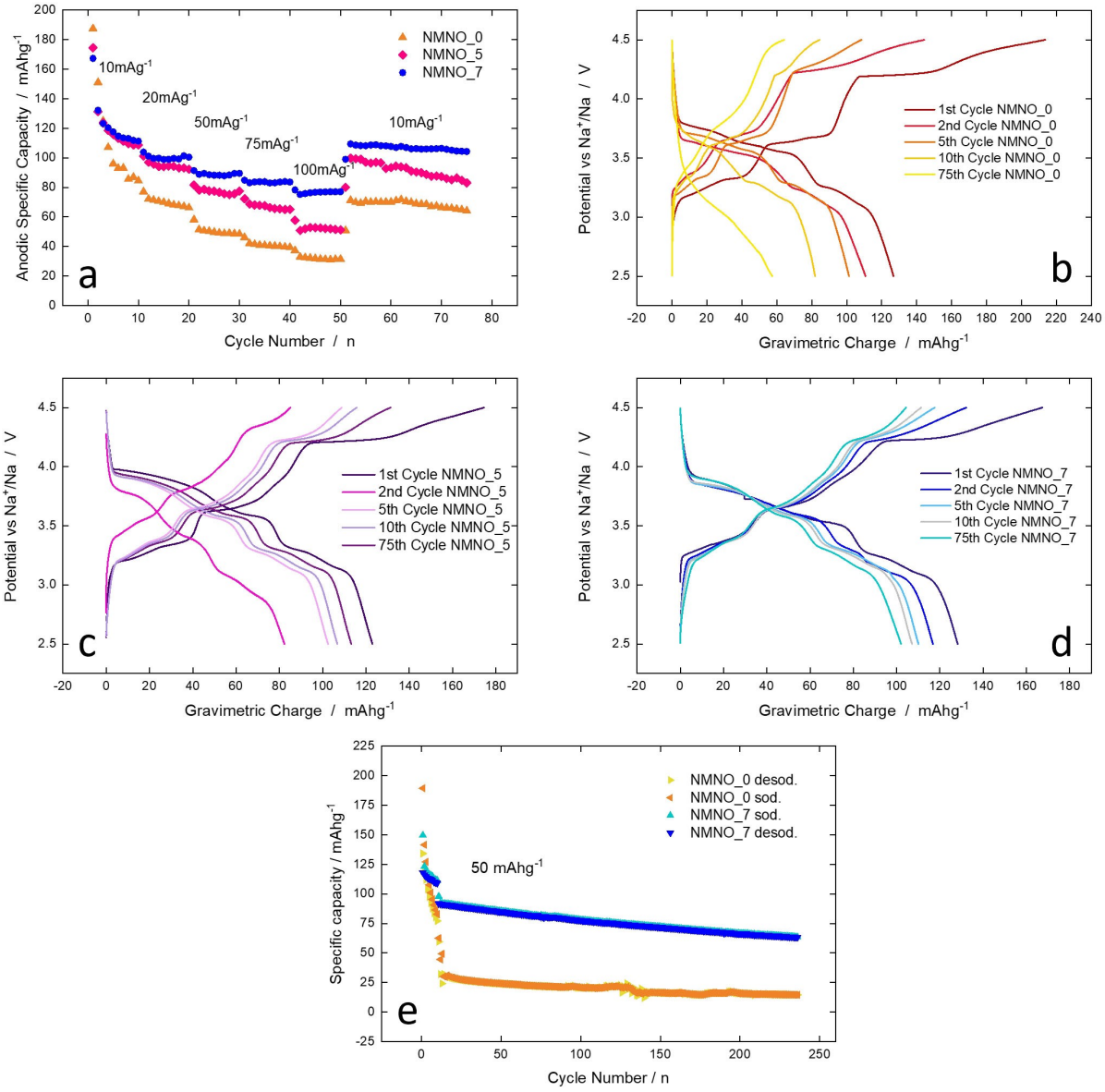

Figure 6. a) Anodic specific capacity and b–d) de-sodiation/sodiation of NMNO samples; e) long cycling analysis.

Research Article
doi.org/10.1002/batt.202300332
Chemistry Europe
European Chemical Societies Publishing

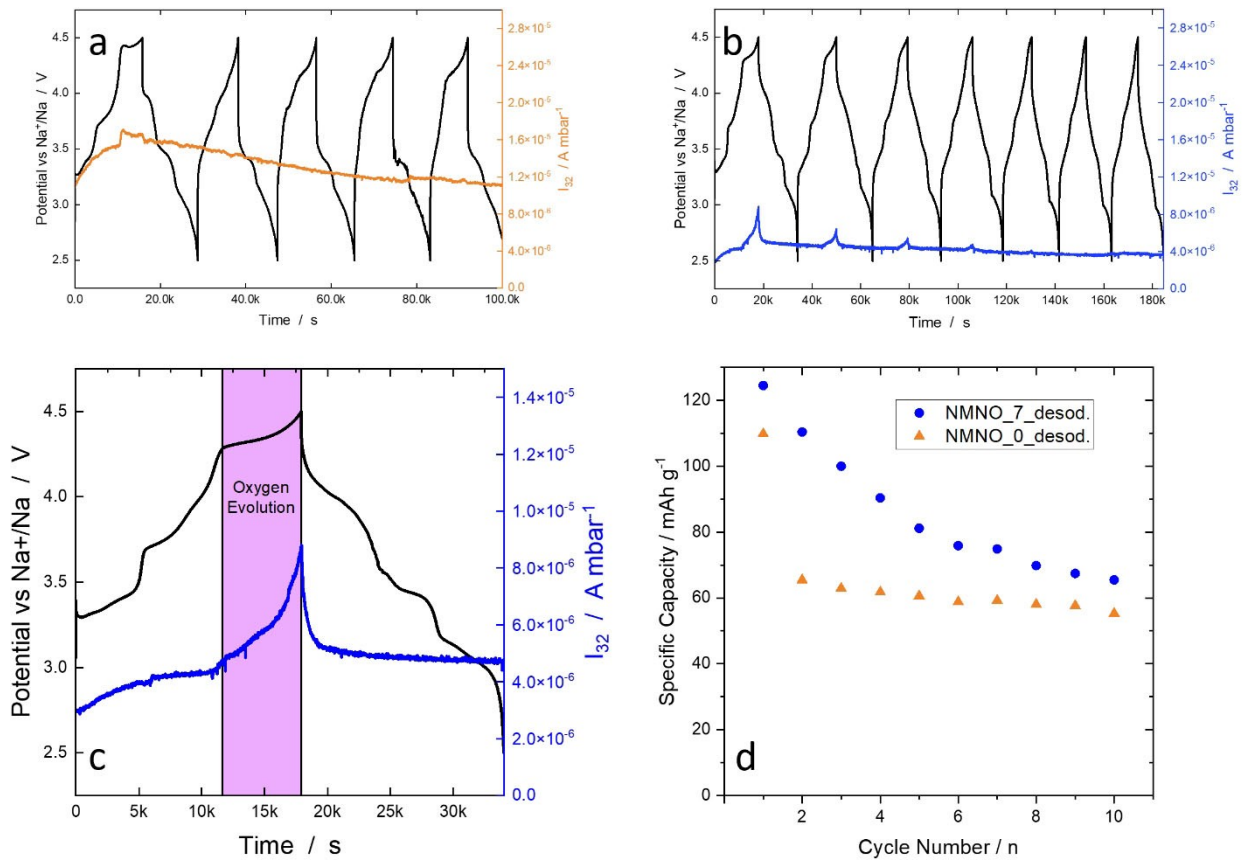

Figure 7. DEMS analysis of NMNO_7. Oxygen production registered in the first de-sodiation/sodiation cycles for the sample a) NMNO_0 and b) NMNO_7. c) Detail of the first cycle of NMNO_7 and d) specific capacity values obtained in the test.

oxidation is immediately removed by the gas flowing through the cell, the decomposition reactions are inevitably irreversible. After the first cycle, the electrochemical reactivity of the material is evidently impaired, as reflected by the complete absence of the plateau at ~4.3 V and the consistent decay of the specific capacity.

A different behavior was observed for the coated material (Figure 7b, c). Indeed, in this case the oxygen production was detected at potential values higher than 4.3 V, but for at least five cycles of the electrochemical testing. The intensity of the peaks progressively decreased, thus demonstrating that the material stabilized or passivated its surface more gradually than the uncoated sample. The fact that oxygen was produced not only in the first cycle could be attributed to an enhanced reversibility of the oxygen reactivity in the system, since the coating layer could make oxygen de-coordination much more complicated. While the oxygen production detected in the NMNO_0 sample led so to a drastic decay in the performance, the NMNO_7 sample showed how the coating could limit the specific capacity decay through the protection of the surface of the cathodic particles.

The capacity retention exhibited vy NMNO_7 was higher than that exhibited by the NMNO_0 sample. While in the first cycle 124 mAh g^{-1} were obtained, the subsequent cycles permitted to achieve cathodic specific capacity values >100 mAh g^{-1}, thus demonstrating that the surface of the material was still able to react properly with Na-ions present in the electrolyte (Figure 7d). In this case, in the NMNO_7 materials the oxygen production was attributed to the presence of areas of the sample in which the coating was not homogeneous, as previously discussed. It must be considered that the stability upon cycling showed in this case by the material was lower than the one previously exhibited during the rate test or the long cycling tests, due to the open cell setup used in this analysis. Nevertheless, the coated and uncoated materials exhibited quite the same capacity decay trend, thus confirming the consistency of the redox behavior of both samples.

Conclusions

MgO-coated P'2-$Na_{0.67}Mn_{0.67}Ni_{0.33}O_2$ system was successfully synthesized with an easily scalable wet chemistry method. The good outcome of the coating procedure was demonstrated by means of XRD and SEM. This last technique showed how the coating agent is creating a rough layer on the cathodic particles. Systematic electrochemical investigation of the considered samples demonstrates the effect of the coating on the stabilization of the electrochemical performances of Ni doped NMO at high potentials, improving both the specific capacity and the mean operating potential. In particular the coating method here presented allows achieving a stable specific

capacity of over 90 mAh g^{-1} at 50 mA g^{-1}, with an operating voltage of 3.66 V vs. Na$^+$/Na, obtaining thus a high-voltage and stable candidate for sodium-ion batteries. Moreover, the high-potential decomposition mechanism of the material was confirmed also by means of DEMS, determining how, in the coated material, oxygen evolution occurs just in the first cycles without compromising the electrochemical reactivity and performances.

Supporting Information

Supporting information contains the experimental details for samples preparation and data acquisition. It also features two figures relative to SEM/EDX analyses on NMNO particles and a figure related to the impedance of NMNO_0 and NMNO_7 at OCV. The authors have cited additional references within the Supporting Information.[56–58]

Acknowledgements

This work has been financed by the Italian Ministry of University and Research (MIUR) through grant PRIN 2017 "Towards sustainable, high-performing, all-solid-state sodium-ion batteries" and carried out within the MOST – Sustainable Mobility Center and received funding from the European Union Next-Generation EU (PIANO NAZIONALE DI RIPRESA E RESILIENZA (PNRR) – MISSIONE 4 COMPONENTE 2, INVESTIMENTO 1.4 – D.D. 1033 17/06/2022, CN00000023). This manuscript reflects only the authors' views and opinions, neither the European Union nor the European Commission can be considered responsible for them. This work was also supported by grant PID2019-107468RB-C21 funded by MCIN/AEI/10.13039/501100011033 and Gobierno Vasco/Eusko Jaurlaritza (project IT1546-22).

Conflict of Interests

The authors declare no conflict of interest.

Data Availability Statement

The data that support the findings of this study are available from the corresponding author upon reasonable request.

Keywords: sodium-ion batteries · sodium layered oxides · differential electrochemical mass spectrometry · inorganic coating

[1] C. Xu, Q. Dai, L. Gaines, M. Hu, A. Tukker, B. Steubing, *Commun. Mater.* **2020**, *1*, 1–10.
[2] Y. Yang, E. G. Okonkwo, G. Huang, S. Xu, W. Sun, Y. He, *Energy Storage Mater.* **2021**, *36*, 186–212.
[3] C. Santos, F. La Mantia, *Curr. Opin. Electrochem.* **2022**, *35*, 101089.
[4] S. E. Can Sener, V. M. Thomas, D. E. Hogan, R. M. Maier, M. Carbajales-Dale, M. D. Barton, T. Karanfil, J. C. Crittenden, G. L. Amy, *ACS Sustainable Chem. Eng.* **2021**, *9*, 11616–11634.
[5] C. B. Tabelin, J. Dallas, S. Casanova, T. Pelech, G. Bournival, S. Saydam, I. Canbulat, *Miner. Eng.* **2021**, *163*, 106743.
[6] T. P. Narins, *Extr. Ind. Soc.* **2017**, *4*, 321–328.
[7] H. S. Hirsh, Y. Li, D. H. S. Tan, M. Zhang, E. Zhao, Y. S. Meng, *Adv. Energy Mater.* **2020**, *10*, 2001274.
[8] C. Vaalma, D. Buchholz, M. Weil, S. Passerini, *Nat. Rev. Mater.* **2018**, *3*, 18013.
[9] F. Duffner, M. Wentker, M. Greenwood, J. Leker, *Renewable Sustainable Energy Rev.* **2020**, *127*, 109872.
[10] J. Spector, M. V. Olano, "Chart: Lithium prices are through the roof this year," can be found under http://www.canarymedia.com/articles/batteries/chart-lithium-prices-are-through-the-roof-this-year, **2022**.
[11] M. Garside, "Mine production of lithium worldwide from 2010 to 2022," can be found under http://www.statista.com/statistics/606684/world-production-of-lithium/, **2023**.
[12] "Lithium ion battery market, Asian players to support European growth," can be found under http://www.sustainable-bus.com/news/lithium-ion-battery-market-asian-players-to-support-european-growth/, 2019.
[13] "Lithium," can be found under https://tradingeconomics.com/commodity/lithium, **2023**.
[14] N. Ortiz-Vitoriano, N. E. Drewett, E. Gonzalo, T. Rojo, *Energy Environ. Sci.* **2017**, *10*, 1051–1074.
[15] J. Jin, Y. Liu, X. Zhao, H. Liu, S. Deng, Q. Shen, Y. Hou, H. Qi, X. Xing, L. Jiao, J. Chen, *Angew. Chem. Int. Ed.* **2023**, *62*, e202219230.
[16] Q. Shen, Y. Liu, X. Zhao, J. Jin, Y. Wang, S. Li, P. Li, X. Qu, L. Jiao, *Adv. Funct. Mater.* **2021**, *31*, 2106923.
[17] Q. Shen, Y. Liu, L. Jiao, X. Qu, J. Chen, *Energy Storage Mater.* **2021**, *35*, 400–430.
[18] Y. F. Liu, K. Han, D. N. Peng, L. Y. Kong, Y. Su, H. W. Li, H. Y. Hu, J. Y. Li, H. R. Wang, Z. Q. Fu, Q. Ma, Y. F. Zhu, R. R. Tang, S. L. Chou, Y. Xiao, X. W. Wu, *InfoMat* **2023**, *5*, e12422.
[19] D. H. Lee, J. Xu, Y. S. Meng, *Phys. Chem. Chem. Phys.* **2013**, *15*, 3304–3312.
[20] Z. Lu, J. R. Dahn, *J. Electrochem. Soc.* **2001**, *148*, A1225.
[21] Y. Zhang, M. Wu, J. Ma, G. Wei, Y. Ling, R. Zhang, Y. Huang, *ACS Cent. Sci.* **2020**, *6*, 232–240.
[22] P.-F. Wang, Y. You, Y.-X. Yin, Y.-S. Wang, L.-J. Wan, L. Gu, Y.-G. Guo, *Angew. Chem.* **2016**, *128*, 7571–7575.
[23] G. Singh, N. Tapia-ruiz, J. Miguel, U. Maitra, J. W. Somerville, A. R. Armstrong, J. M. De Ilarduya, P. G. Bruce, *Chem. Mater.* **2016**, *28*, 5087–5094.
[24] B. Peng, G. Wan, N. Ahmad, L. Yu, X. Ma, G. Zhang, *Adv. Energy Mater.* **2023**, *13*, 2300334.
[25] D. Pahari, A. Kumar, D. Das, S. Puravankara, *Int. J. Energy Res.* **2022**, *46*, 21894–21927.
[26] Y. Liu, X. Fang, A. Zhang, C. Shen, Q. Liu, H. A. Enaya, C. Zhou, *Nano Energy* **2016**, *27*, 27–34.
[27] J. Alvarado, C. Ma, S. Wang, K. Nguyen, M. Kodur, Y. S. Meng, *ACS Appl. Mater. Interfaces* **2017**, *9*, 26518–26530.
[28] K. Tang, Y. Huang, X. Xie, S. Cao, L. Liu, M. Liu, Y. Huang, *Chem. Eng. J.* **2020**, *384*, 123234.
[29] C. H. Jo, J. Jo, H. Yashiro, S. Kim, Y. Sun, *Adv. Energy Mater.* **2018**, *8*, 1702942.
[30] G. Shao, W. Kong, Y. Yu, J. Zhao, W. Yang, J. Yang, Y. Li, X. Liu, *Inorg. Chem.* **2023**, *62*, 9314–9323.
[31] Y. Zhou, L. Li, Y. Wu, H. Xie, *Eur. J. Inorg. Chem.* **2023**, *26*, e202200685.
[32] J. Zuo, W. Qiu, J. Liu, X. Ren, F. Liu, H. He, H. Luo, C. Li, Y. Ortiz, G. F. Duan, H. Liu, J. Wang, M. S. Li, Y. Fu, R. Yong, *Nat. Commun.* **2020**, *11*, 1–12.
[33] J. Lamb, A. Manthiram, *Chem. Mater.* **2020**, *32*, 8431–8441.
[34] P. Delmas, C. Fouassier, P. Hagenmuller, *Physica* **1980**, *99B*, 81–85.
[35] L. Zhang, J. Wang, J. Li, G. Schuck, M. Winter, G. Schumacher, J. Li, *Nano Energy* **2020**, *70*, 104535.
[36] N. Yabuuchi, S. Komaba, *Sci. Technol. Adv. Mater.* **2014**, *15*, 043501.
[37] Y. Lei, X. Li, L. Liu, G. Ceder, *Chem. Mater.* **2014**, *26*, 5288–5296.
[38] P. Gupta, S. Pushpakanth, M. A. Haider, S. Basu, *ACS Omega* **2022**, *7*, 5605–5614.
[39] Y. You, A. Dolocan, W. Li, A. Manthiram, *Nano Lett.* **2019**, *19*, 182–188.
[40] Q. Xie, W. Li, A. Manthiram, *Chem. Mater.* **2019**, *31*, 938–946.
[41] X. Liu, S. Wang, L. Wang, K. Wang, X. Wu, P. Zhou, Z. Miao, J. Zhou, Y. Zhao, S. Zhuo, *J. Power Sources* **2019**, *438*, 227017.

[42] K. Wang, H. Wan, P. Yan, X. Chen, J. Fu, Z. Liu, H. Deng, F. Gao, M. Sui, *Adv. Mater.* **2019**, *31*, 1–10.
[43] R. J. Clément, J. Billaud, A. Robert Armstrong, G. Singh, T. Rojo, P. G. Bruce, C. P. Grey, *Energy Environ. Sci.* **2016**, *9*, 3240–3251.
[44] J. Li, H. Li, W. Stone, R. Weber, S. Hy, J. R. Dahn, *J. Electrochem. Soc.* **2017**, *164*, A3529–A3537.
[45] H. Li, J. Li, X. Ma, J. R. Dahn, *J. Electrochem. Soc.* **2018**, *165*, A1038–A1045.
[46] I. Hasa, D. Buchholz, S. Passerini, B. Scrosati, J. Hassoun, *Adv. Energy Mater.* **2014**, *4*, 1400083.
[47] H. Yoshida, N. Yabuuchi, K. Kubota, I. Ikeuchi, A. Garsuch, M. Schulz-Dobrick, S. Komaba, *Chem. Commun.* **2014**, *50*, 3677–3680.
[48] Y. Liu, J. Harlow, J. Dahn, *J. Electrochem. Soc.* **2020**, *167*, 020512.
[49] M. Mou, A. Patel, S. Mallick, K. Jayanthi, X. G. Sun, M. P. Paranthaman, S. Kothe, E. Baral, S. Saleh, J. H. Mugumya, M. L. Rasche, R. B. Gupta, H. Lopez, M. Jiang, *ACS Appl. Energ. Mater.* **2022**, *6*, 3213–3224.
[50] X. Luo, X. Wang, L. Liao, S. Gamboa, P. J. Sebastian, *J. Power Sources* **2006**, *158*, 654–658.
[51] W. Hua, J. Zhang, Z. Zheng, W. Liu, X. Peng, X. D. Guo, B. Zhong, Y. J. Wang, X. Wang, *Dalton Trans.* **2014**, *43*, 14824–14832.
[52] K. Kaliyappan, W. Xaio, T.-K. Sham, X. Sun, *Adv. Funct. Mater.* **2018**, *28*, 1801898.
[53] C. H. Jo, J. H. Jo, H. Yashiro, S. J. Kim, Y. K. Sun, S. T. Myung, *Adv. Energy Mater.* **2018**, *8*, 1702942.
[54] A. Bani Hashemi, F. La Mantia, *Anal. Chem.* **2016**, *88*, 7916–7920.
[55] M. Tribbia, J. Glenneberg, G. Zampardi, F. La Mantia, *Batteries & Supercaps* **2022**, *5*, e202100381.
[56] J. Lamb, K. Jarvis, A. Manthiram, *Small* **2022**, *18*, 2106927.
[57] A. Ponrouch, E. Marchante, M. Courty, J. M. Tarascon, M. R. Palacín, *Energy Environ. Sci.* **2012**, *5*, 8572–8583.
[58] G. Åvall, J. Mindemark, D. Brandell, P. Johansson, *Adv. Energy Mater.* **2018**, *8*, 1–22.

Manuscript received: July 26, 2023
Revised manuscript received: October 11, 2023
Accepted manuscript online: October 16, 2023
Version of record online: October 27, 2023